DOI: 10.13009/EUCASS2023-041
Aerospace Europe Conference 2023 – 10TH EUCASS – 9TH CEAS

# Optical investigation of paraffin-based fuel combustion in a hybrid rocket slab burner

*Riccardo Gelain*[1,⋆], *Artur Elias De Morais Bertoldi*[1,2], *Patrick Hendrick*[1] *and Michel Lefebvre*[3]
[1]*Université Libre de Bruxelles, Aero-Thermo-Mechanics Department,*
*50 Avenue F.D. Roosevelt, 1050 Brussels, Belgium*
[2]*University of Brasilia, Chemical Propulsion Laboratory,*
*AE Indústria Projeção A, 72.444-240 Gama, Brazil*
[3]*Royal Military Academy*
*30 Avenue de la Renaissance, 1000 Brussels, Belgium*
riccardo.gelain@ulb.be
⋆Corresponding author

## Abstract

Hybrid rocket slab burners can be used to study the combustion behaviour of different hybrid rocket fuels at different operating conditions thanks to optical accesses and high-speed video techniques. This paper focuses on the combustion visualization of a paraffin-based fuel grain burning with oxygen at different pressure and oxidizer mass flux. After a short overview of the experimental setup and the improvements over previous works, some images acquired during two different test campaign are shown, and the main features of paraffin combustion identified in the videos are discussed. Finally, a qualitative discussion of the effect of the pressure and oxidizer mass flux on the observed flame thickness and brightness is provided.

## 1. Introduction

Hybrid rocket engines (HREs) are a category of chemical rocket propulsion systems in which the two propellants are stored in different states of matter. Being often overlooked for their lower performance with respect to conventional liquid rocket engines, and increased complexity over solid rocket motors, they are recently gaining new momentum for small launchers applications, as their satisfying performance is coupled with intrinsic safety, throttle-ability, flexibility and low cost. To study and develop models of the internal ballistics of a HRE, combustors with optical access, or hybrid rocket slab burners, can be employed to visualize the flame and understand the physical phenomena that take place in a combustion chamber. Using high-speed videos, flame and boundary layer thickness of different fuels at different operating conditions can be investigated,[1–3] the effect of viscosity of the burning liquid layer can be identified,[4–6] as well as the entrainment of paraffin droplets.[7,8] A hybrid rocket slab burner has been recently developed at Université Libre de Bruxelles (ULB), to increase the research capabilities of the department and to work in synergy with the main 1kN Hybrid Rocket Engine. The design of the test facility, named MOUETTE (Moteur OptiqUe pour ÉTudier et Tester Ergols hybrides), has been validated during a preliminary commissioning test campaign.[9] The main design driver behind the development was the conception of a small combustion chamber that could be used to preliminary investigate the performance of solid fuels before testing them in the larger scale HRE. The combustion images acquired using a high-speed camera have then been used for the preliminary development of a numerical technique to estimate the regression rate evolution over time through image processing.[10] This paper takes on from the previous research performed with the MOUETTE burner to focus on what has been observed using a high-speed camera to visualize the flame behaviour in the chamber. After an overview of the design tweaks that have been introduced in order to improve the efficacy and quality of the data acquired from the tests, more focus is given to the images acquired over two different test campaigns, to discuss the main qualitative features of paraffin combustion that have been identified in the experiments.

## 2. Experimental Setup

The MOUETTE slab burner design rationale is detailed in a previous work of the authors.[9] The combustor features a modular design, so the components can be modified according to the different research needs. The selected oxidizer

DOI: 10.13009/EUCASS2023-041



is gaseous oxygen, with a mass flow rate that can be adjusted using a chocking orifice in the feed lines and varying the pressure of the gas fed from the reservoir. The ignition of the solid fuel slab is achieved with a pyrotechnic squib, and the pressure in the combustion chamber is maintained using a convergent nozzle with a graphite throat insert. Pressure measurements are acquired both in the combustion chamber and in the feed lines, as well as the oxygen flow temperature. The combustion chamber has two parallel quartz windows that can be used to perform high-speed video acquisitions, also with chemiluminescence and schlieren imaging techniques. For the tests investigated in this paper, a Photron FASTCAM SA4 high-speed camera has been used. The maximum operating conditions of the MOUETTE slab burner are listed in Table 1 while a photograph of a test is shown in Figure 1.

Table 1: Maximum operating conditions of MOUETTE

| | | |
|---|---|---|
| Combustion Chamber Pressure | 10 | bar |
| Oxidizer Mass Flow Rate | 100 | g/s |
| Oxidizer Mass Flux | 50 | kg/m$^2$s |
| Burn Time | 10 | s |

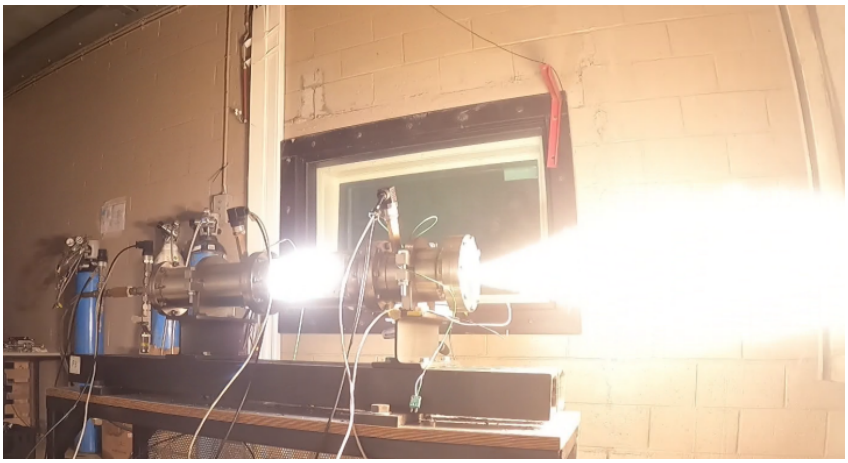

Figure 1: Photograph of a MOUETTE test at high pressure conditions

### 2.1 Feed system calibration

The oxygen mass flow rate is metered using a chocking orifice, positioned upstream of the combustor injector head. In particular, knowing the pressure and temperature of the gas upstream of the orifice, the mass flow rate of gas can be calculated according to the following equation:

$$\dot{m} = c_D A \sqrt{\gamma \rho_0 P_0 \left(\frac{2}{\gamma+1}\right)^{\frac{\gamma+1}{\gamma-1}}} \tag{1}$$

Where $\dot{m}$ is the oxygen mass flow rate, $\gamma$ the heat capacity ratio of oxygen and $\rho_0$ its density upstream of the orifice, $P_0$ the pressure of the flow upstream of the orifice, $A$ the area of the orifice and $c_D$ the discharge coefficient. In general, once the discharge coefficient value is known, the mass flow rate of oxidizer can be set just by adjusting the orifice diameter and regulating the pressure upstream of it with the pressure regulator. An accurate value of the mass flow can then be calculated after the test, as the pressure and the temperature are measured. To increase the flexibility of the system, three different orifices have been manufactured and calibrated, measuring the mass flow rate of a nitrogen flow injected through the orifice at different feeding pressures. The diameters and the resulting value of the discharge coefficient are listed in Table 2, while the experimental results of the calibration are shown in Figure 2.

Table 2: Choking orifice diameters and discharge coefficient

| | | | |
|---|---|---|---|
| Orifice Diameter | 1.9 mm | 2.4 mm | 2.7 mm |
| Discharge Coefficient | 0.6 | 0.6 | 0.6 |

DOI: 10.13009/EUCASS2023-041



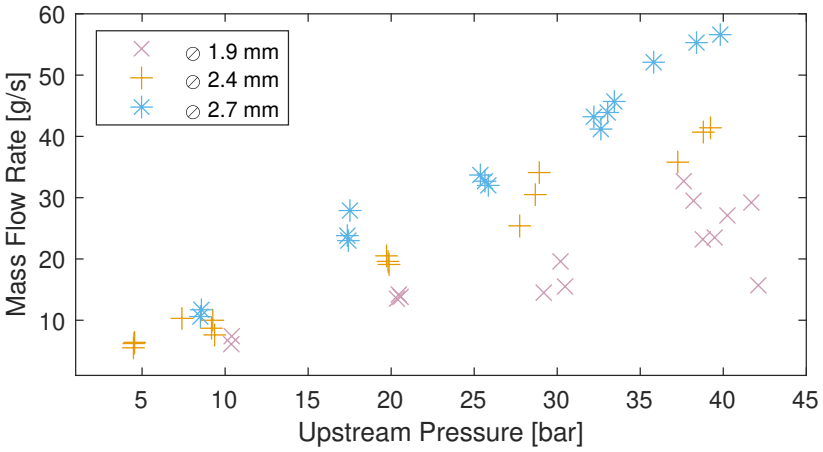


Figure 2: Mass flow rate against upstream gauge pressure for the choking orifice

### 2.2 Fuel slab dimensions

The typical slab burner fuel sample is a slab with a right-angled trapezoid section, with a forward facing ramp that acts as flameholder. The slope angle affects the behavior of the combustion: Petrarolo et al.,[11] observed that a ramp too shallow doesn't hold the flame, while a ramp too steep induces a vortex shedding phenomena, that may also generate combustion instabilities, as witnessed also by Jens et al.[3] Two types of slabs have been used in the experiments described in this paper. The first version, used in the commissioning campaign, has a 60° ramp angle, an average length of 100mm, width of 40 mm and height of 30 mm, shown in Figure 3.a. As an improvement over the first version, a second type of slab has then been realized for the second test campaign, called Phase 2 in this paper, shown in Figure 3.b, with the objectives of decreasing the vortex shedding at the leading edge, of reducing the lateral burning, and increasing the burning area, to reduce the oxidizer to fuel ratio. In particular, a lower ramp angle has been selected (30°), and a larger thickness has been introduced, to fill the distance between the two windows, to reducing the amount of flame structures developing on the side of the slab. The new slab is on average 125 mm long, 75 mm wide and 30 mm high, presenting a larger surface exposed to the oxidizer flow. The properties are summarized in Table 3, while two photographs are shown in Figure 3. Few tests with an intermediate fuel grain, with a width of 56 mm, have been done, to assess the effect of the gap between the slab and the glass of the optical accesses on the quality of the high-speed videos recorded.

Table 3: MOUETTE fuel slab characteristics

| | **Commissioning** | **Phase 2** |
|---|---|---|
| Base Length | 100 mm | 125 mm |
| Width | 40 mm | 75 mm |
| Height | 30 mm | 30 mm |
| Ramp Angle | 60° | 30° |

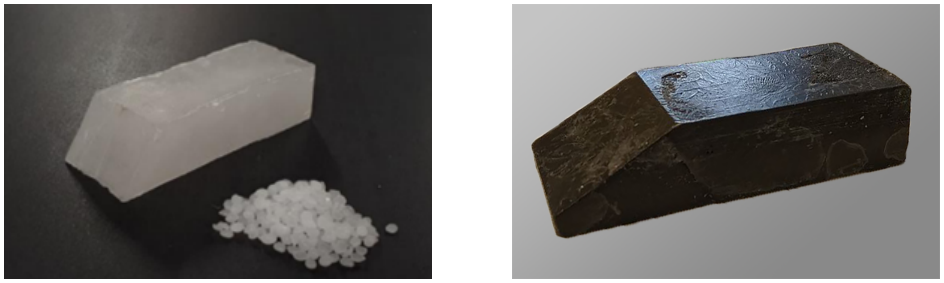

(a) Commissioning campaign slab

(b) Phase 2 slab

Figure 3: Paraffin fuel slabs

DOI: 10.13009/EUCASS2023-041



# 3. Experimental Results

## 3.1 Tests Overview

The tests investigated in this paper are a selection of results taken from two tests campaign conducted with the MOUETTE slab burner. The first dataset comes from the commissioning campaign, which has been discussed by the authors in a previous work, but only few images of the combustion had been disclosed.[9] The overview of the tests that will be analysed in this paper and the average value of the test parameters is given in Table 4, where the original enumeration has been kept. For clarity, the commissioning test number is denoted by a "C", to distinguish them from the other tests described in the paper. The pressure value indicated is the gauge pressure. All the test listed has been performed with the smaller fuel slab described in Section 2.2. The propellant used is pure paraffin (Tudamelt 52/54 supplied by H&R). As these tests are taken from the first experimental campaign, where the main objective was the validation of the test setup design, therefore a wide range of test conditions have been tested, varying both the mass flow rate and the chamber pressure, the test duration and the igniter mass, but keeping the fuel grain dimensions and composition constant. The campaign was used also to learn and improve the quality of the high-speed video acquisition, testing different camera configurations, in particular the frame rate, shutter speed and lens aperture, and filters for OH* and CH* chemiluminescence have been tested as well. For these reasons, few videos can be fully exploited to analyse the combustion behavioour of the paraffin slab. The tests with data acquisition errors or performed with metallic additives or unconventional geometries have also been omitted. The camera parameters are listed in Table 5.

Table 4: Commissioning test campaign overview

| Test Number [-] | Burn Time [s] | Tank Pressure [bar] | Chamber Pressure [bar] | Mass Flow [g/s] | Mass Flux [kg/m$^2$s] |
|---|---|---|---|---|---|
| C-09 | 5.25 | 37.22 | 2.88 | 32.60 | 10.13 |
| C-11 | 5.52 | 34.92 | 2.23 | 48.72 | 15.14 |
| C-12 | 5.61 | 34.86 | 2.28 | 48.56 | 15.09 |
| C-19 | 5.46 | 35.00 | 2.04 | 59.20 | 18.40 |
| C-20 | 5.56 | 33.46 | 4.76 | 58.87 | 18.30 |

Table 5: Commissioning test campaign video parameters

| Test Number | Frames per Second | Lens Aperture | Shutter Speed | Resolution | Filter |
|---|---|---|---|---|---|
| C-09 | 3000 | f11 | 1/3000 | 768x512 | None |
| C-11 | 3000 | f11 | 1/3000 | 768x512 | CH* |
| C-12 | 3000 | f11 | 1/3000 | 768x512 | CH* |
| C-19 | 6000 | f11 | 1/6000 | 512x352 | CH* |
| C-20 | 6000 | f11 | 1/6000 | 512x352 | CH* |

The second test batch that has been taken into account for this research is from a more recent campaign, where the fuel slab with the ramp angle of 30° has been used. An overview of the tests analyzed in this paper is given in Table 6. Different widths of the sample have been tried to evaluate the impact of the flame developing on the sides on the quality of the videos, and the camera parameters have been adjusted to compensate the brightness of the flame. In particular, Test 03 has the 56 mm wide fuel slab. The omitted tests present low quality images (videos underexposed or overexposed), a leak or an issue with the data acquisition. The camera parameters used for the second batch of videos are listed in Table 7.

Table 6: Phase 2 test campaign overview

| Test Number [-] | Burn Time [s] | Tank Pressure [bar] | Chamber Pressure [bar] | Mass Flow [g/s] | Mass Flux [kg/m$^2$s] |
|---|---|---|---|---|---|
| 03 | 5.11 | 31.56 | 0.09 | 27.78 | 10.59 |
| 04 | 3.99 | 30.27 | 0.07 | 26.75 | 13.04 |
| 08 | 3.51 | 34.39 | 9.02 | 59.81 | 29.15 |
| 12 | 3.98 | 32.71 | 10.14 | 57.95 | 28.24 |
| 14 | 5.18 | 36.79 | 0.26 | 31.82 | 15.51 |

DOI: 10.13009/EUCASS2023-041



Table 7: Phase 2 test campaign video parameters

| Test Number | Frames per Second | Lens Aperture | Shutter Speed | Resolution | Filter |
|---|---|---|---|---|---|
| 03 | 2000 | f8 | 1/593000 | 896x512 | None |
| 04 | 2000 | f8 | 1/593000 | 896x512 | None |
| 08 | 2000 | f16 | 1/593000 | 896x512 | None |
| 12 | 2000 | f16 | 1/593000 | 896x512 | None |
| 14 | 2000 | f8 | 1/593000 | 896x512 | None |

The oxidizer mass flow indicated in the tables has been calculated with the new calibration of the discharge coefficient, bringing a correction over the values listed in the previous work.[9] The oxidizer mass flux $G_{ox}$ indicated is calculated as follows:

$$G_{ox} = \frac{\dot{m}_{ox}}{A_p - h_g w_g} \tag{2}$$

Where the numerator is the oxidizer mass flow rate $\dot{m}_{ox}$ and the denominator is the cross-section of the combustion chamber traversed by the gas flow: in particular, $A_p$ is the empty section of the chamber, minus the section of the fuel slab normal to the flow direction, calculated using the height $h_g$ and the width $w_g$. As the fuel consumption is small compared to the total cross section of the test chamber, the variation induced by the fuel consumption is neglected for this preliminary discussion, therefore the oxidizer mass flux at the average measured oxidizer mass flow but with the initial geometrical dimensions is considered. For clarification, a CAD sketch of the test chamber cross section with the fuel slab is shown in Figure 4. A striped pattern is used to visually highlight the cross-section used for the $G_{ox}$ estimation.

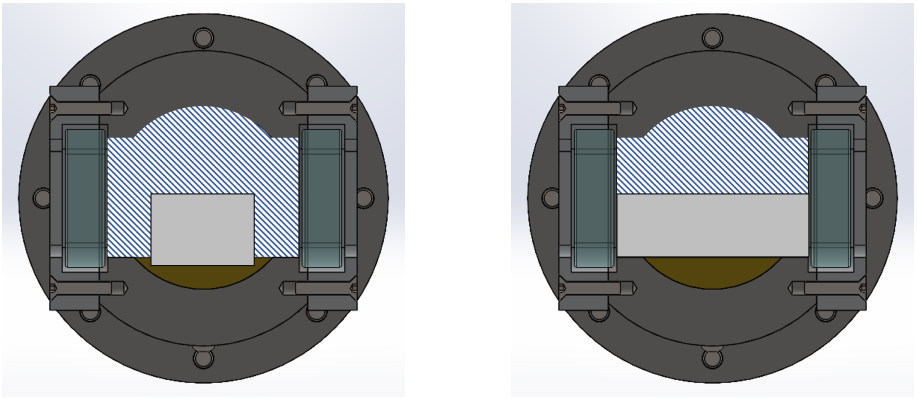

(a) Commissioning test (b) Phase 2 test

Figure 4: Cross-section for $G_{ox}$ evaluation

### 3.2 Main Combustion Features

A typical example of the slab combustion process that can be visualized in the MOUETTE is given in Figures 5 and 6. In particular, the image on the left is a snapshot of the test taken during the main combustion phase, while the image on the right is the average light intensity calculated over 0.5 seconds (1000 frames). The fuel slab trapezoidal shape can be discerned in both figures, with the forward facing ramp of the leading edge on the left side. The oxidizer is flowing from left to right. As the test section is not illuminated, all the light that is captured by the high-speed camera comes from the flame itself. Therefore, the trailing edge of the slab is harder to detect due to the recirculation zone that forms after the backward facing step. Test 08 is characterized by a higher $G_{ox}$ and combustion chamber pressure, which translates in a brighter and more developed flame, as can be seen by comparing the figures. The averaged images help also to visually recognize the different thickness of the flame core. In Figure 6 is also possible to see some flame structures developing on the side of the fuel slab, attached to the leading edge, as well as a flame developing on the bottom of the photograph, induced by a melted layer of paraffin which falls on the bottom of the test section and burns in the gap between the fuel slab and the glass. In the background, the gasket protecting the rear window can also be seen ablating due to the high temperature. The observed flame structures are highly oscillating. Liu et al.[8] experienced

DOI: 10.13009/EUCASS2023-041



similar combustion oscillations and attributes their insurgence to the periodic accumulation and breakdown of the liquid film layer.

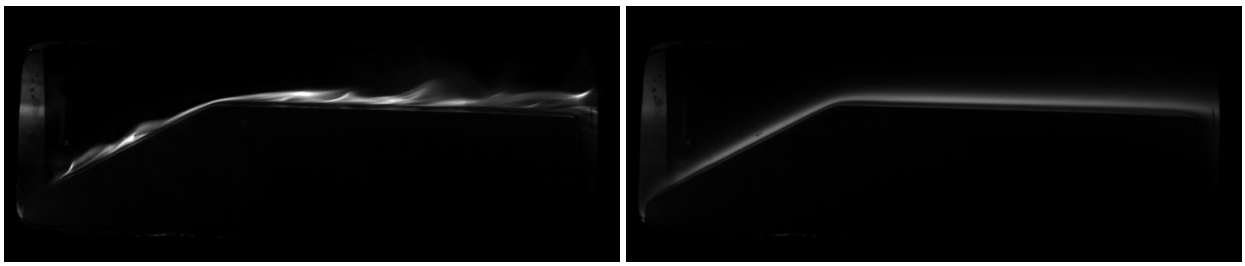

(a) Frame from the test (b) Average intensity

Figure 5: Combustion images of Test 04

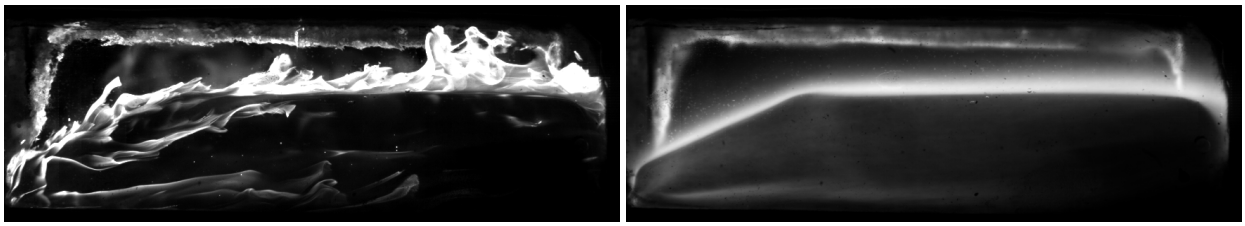

(a) Frame from the test (b) Average intensity

Figure 6: Combustion images of Test 08

A more detailed view of combustion of paraffin on the surface is shown on Figure 7, which gives a closer look to the snapshot of Figure 5. Looking at the figure, the black area on the bottom is the lateral surface of the fuel slab. On top of it there is a narrow bright zone, before a second dark area. The bright zone is assumed to be the liquefied surface of the paraffin slab, which glows reflecting the light of the flame. Between the liquid surface and the flame core there is the fuel rich dark zone, which is filled by the mass flux of gaseous pyrolized fuel coming from the slab surface. Over the flame zone there is a second dark area, which is oxidizer rich and filled by the oxygen mass flow. This diffusive flame structure observed experimentally is in accordance with the theoretical models described in literature.[12]

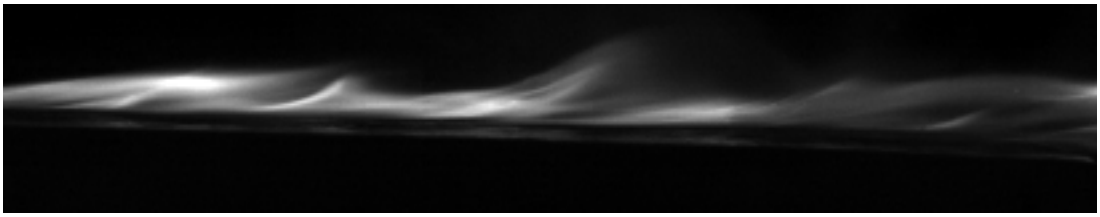

Figure 7: Magnification of a combustion image from Test 04

A typical phenomenon theorized in the combustion of paraffin-based fuels in HREs is the entrainment of liquid fuel droplets in the oxidizer flow. The small droplets couldn't be visualized in the videos gathered. The reasons could be multiple. First, the droplet size could be too small to be captured by the camera. Second, the brightness of the flame saturates the image in proximity of the droplets, which are burning cores themselves, therefore enveloped by a burning surface. Larger liquid droplets can be however visualized in correspondence with local blowing events at the surface of the grain, typically coupled with pressure increases induced by the enhanced instantaneous fuel mass flow. Some photographs, taken from Test 08, are shown in Figure 8 where the burning fuel droplets ejected in the oxidizer flow by some local surface instabilities can be identified. The dark zone that can be seen in the bottom right of the pictures is due to the accumulation of soot on the surface of the glass.

During a test the conditions of the flame change often, presenting higher oscillations and blowing events at higher pressures. The flames transitions from more chaotic behaviour to regular oscillations, suggesting a coupling between the mass and heat release and the pressure in the chamber.

The typical phases that can be observed during a test are the ignition start-up, the nominal combustion regime and the shut-off transient. These phases present a different flame thickness and brightness, and clustering techniques can be

DOI: 10.13009/EUCASS2023-041



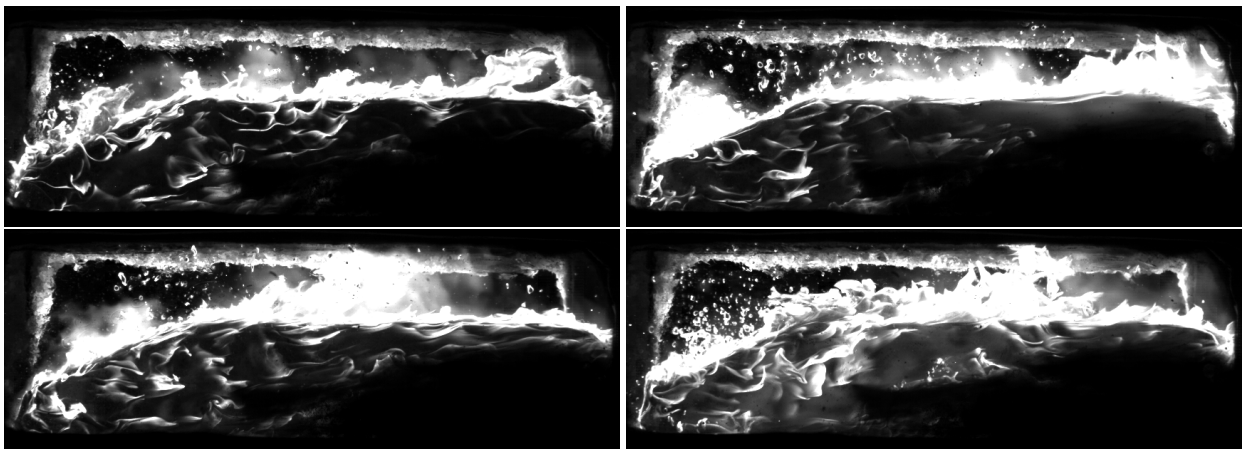

Figure 8: Droplets combustion events observed in Test 08

used to automatically split the videos in the different phases to facilitate the post processing.[13] The three phases are shown together in Figure 9 for comparison. In the ignition phase, the igniter is typically not fully consumed, and the hot gases can be seen on the left of the frame in Figure 9.a, close to the leading edge. The oxygen main valve is opening, and as oxygen begins to flow the flame develops on the surface of the slab. After the combustion regime which is the main part of the test investigated in the research, a frame from the shut-off transient is shown in Figure 9.c. the oxygen valve is closing, therefore the flow of oxygen reduces, the slab cools down and the flame becomes darker, until the total extinction, which is then guaranteed by the flow of nitrogen used to quench the flame and stop the test.

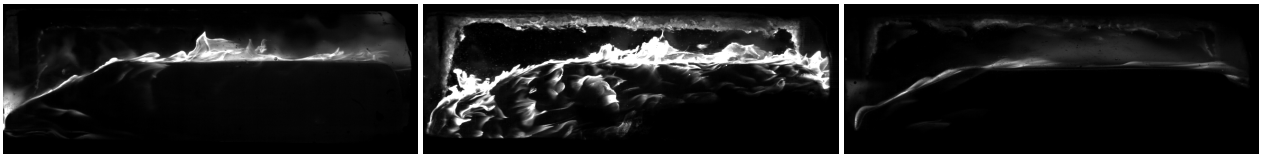

(a) Ignition transient (b) Nominal regime (c) Shut-off transient

Figure 9: Different test phases observed in Test 08

Finally, as can be seen comparing Figures 5 and 6 (or 8), a flame is developing also on the side of the slab, while ideally only the upper surface should burn, as the objective is to experimentally simulate a 2-Dimensional flow. This phenomenon has been observed especially at higher oxidizer mass flow and combustion chamber pressure, when the regression rate of the solid fuel increase. In fact, as the fuel burns also on the lateral side, the gap between the slab and the quartz window increases, reducing the local velocity of the oxygen flow thus enabling a more stable flame, which is anchored to the edge of the slab which acts as flameholder.

### 3.3 Atmospheric Pressure Tests

The main objective of this and the following sections is to provide a deeper insights on the images that have been recorded using the high-speed camera for the commissioning test campaign. Due to the limitation of the medium, only some selected frames are shown, and the qualitative features that can be observed are discussed.

The first tests shown here have been selected from the Phase 2 test campaign. As stated before, this campaign presents several improvements over the commissioning campaign, both in the fuel grain shape and in the quality of the videos, as more experience has been acquired over time.

Tests 03, 04 and 14 have been executed using a nozzle with a large throat, which provides a light backpressure but does not choke during the test, and with the smallest orifice for the oxidizer feed system, thus guaranteeing a small mass flow rate. The resulting pressure in the chamber is close to the atmospheric pressure, slightly higher in test 14 due to the higher feeding pressure, which translated in a higher oxidizer mass flow rate (see Table 6). The oxidizer mass flux between the tests is comparable as well, ranging between 10 and 15 $kg/m^2s$. The images shown in the section have been selected from the main combustion phase, at a burning time of about 3 seconds. The camera settings are the same between the three tests. The contrast of the images has been enhanced to improve the visibility of the flame.

DOI: 10.13009/EUCASS2023-041



The results of Test 03 and 04 are shown in Figures 10 and 11, respectively. The qualitative behaviour observed is very similar, the small difference between the tests is the width of the fuel slab. Test 03 uses the slab of 56 mm width, while the slab of Test 04 is 75 mm wide. this translates in a larger amount of gas flowing on the side, which is partially visible when comparing the frames and burning gas takes the shape of light fog. The effect is even more accentuated by a small portion of the igniter squib trapped on the front of the paraffin slab, which is still burning and releases some gas in the chamber. The igniter is also the cause of the small glowing spots entrained in the oxidizer flow seen on the left side of the frames.

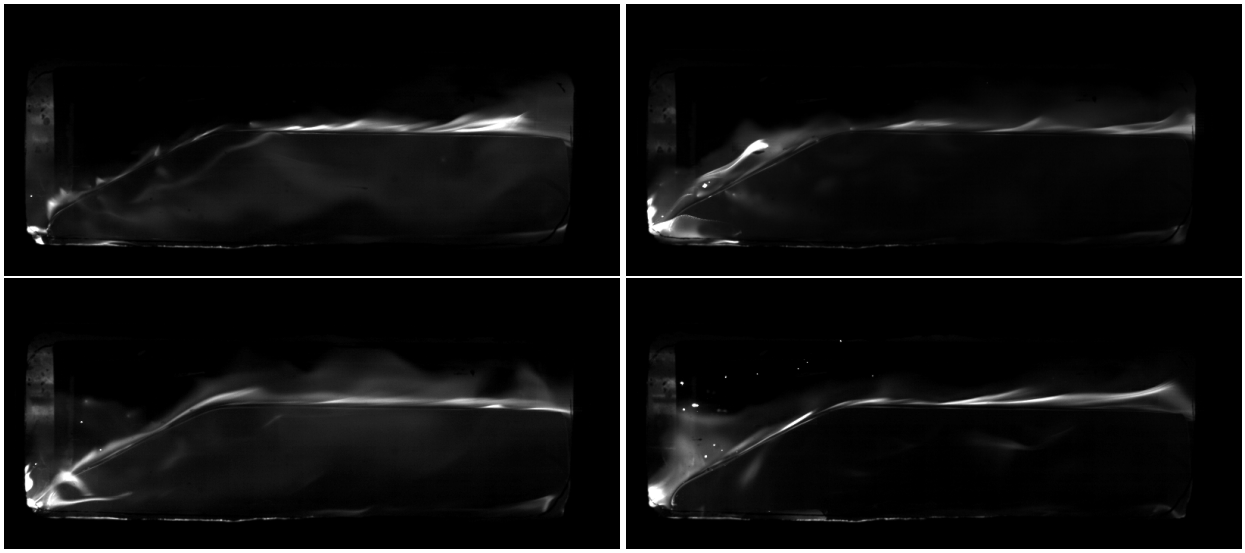

Figure 10: Paraffin combustion of Test 03

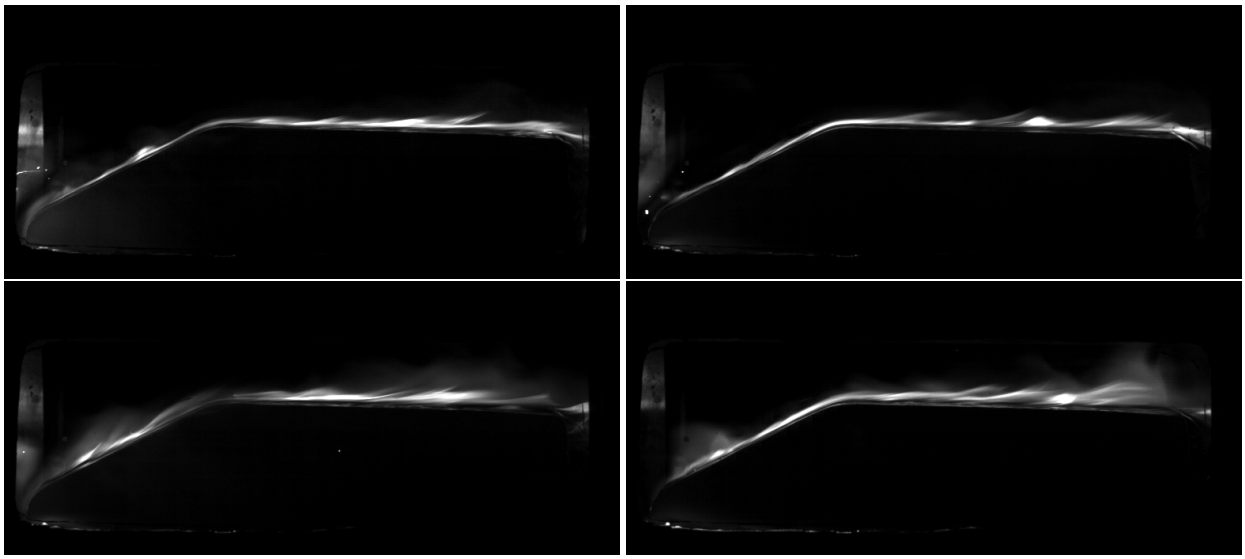

Figure 11: Paraffin combustion of Test 04

Test 14 presents a behaviour similar to Test 04, and is shown in Figure 12. The pressure and mass flux variations between the two cases are too small to visually appreciate the differences between the tests, and qualitatively it present similar results.

Overall, the behaviour observed in the combustion at atmospheric pressure corresponds to the flame structure developing in the ignition phase of higher pressure tests. The low pressure in the chamber and low mass flow rate are in fact a similar condition to what is experienced during the ignition transient, as can be appreciated by comparing the pictures with Figure 9.a.

DOI: 10.13009/EUCASS2023-041



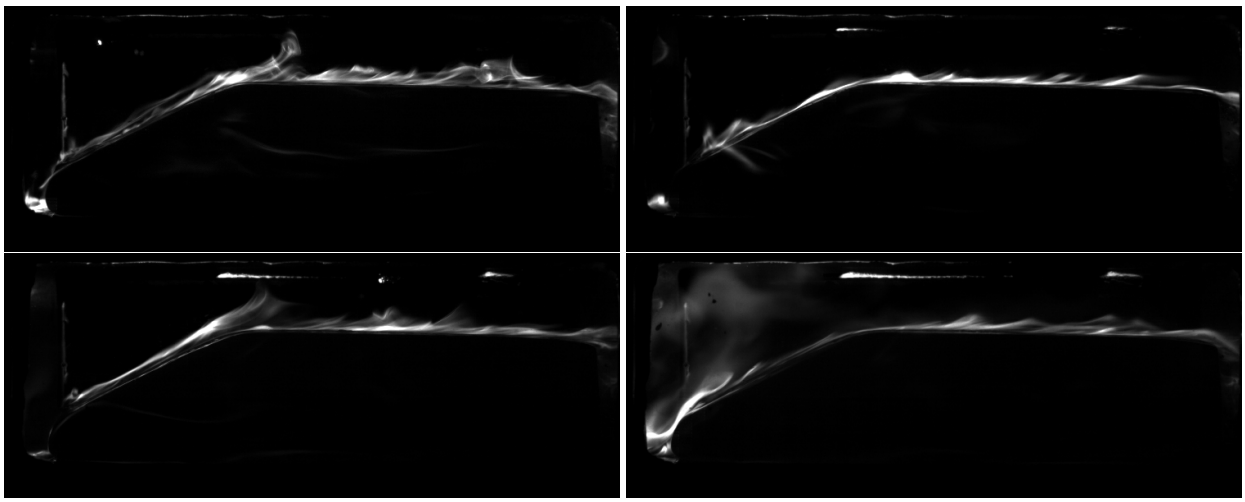

Figure 12: Paraffin combustion of Test 14

### 3.4 Low Pressure Tests

The second batch of tests investigated comes from the commissioning test campaign, in particular test C-09, C-11 and C-12. These tests feature the same oxidizer mass flux of the atmospheric tests shown before, ranging from 10 to 15 kg/m$^2$, but this time a nozzle throat insert with a smaller diameter has been used, to achieve a combustion chamber pressure between 2 and 3 bar gauge. Some images are shown in Figure 13, where the video of Test C-09 has been acquired with a filter for CH* chemiluminescence.

While the fuel slab shape is different and narrower with respect to the tests discussed before, enhancing the onset of a flame on the lateral surface of the fuel slab, a change in the flame thickness and brightness can be appreciated When compared with the atmospheric tests results of the previous section. In particular, the flame appears to be more developed, with a larger thickness and brightness, as well as more visible oscillations and instabilities. Part of the increase in flame thickness may also be induced by the oxidizer flowing on the sides of the slab. While the oxidizer mass flux is the same, the increased chamber pressure acts on the heat exchange ratio at the fuel surface, increasing the regression rate and the local fuel evaporation, resulting in the brighter and thicker flame profile observed.

Test C-19 is grouped together with test C-20 as the camera settings used between the tests are the same, with an increase in the frame rate and shutter speed. Some frames are shown in Figure 14. The two tests have the same oxidizer mass flux, of around 18 kg/m$^2$, higher then the previous tests, but two different pressure values, 2 bar for test C-19 and around 5 bar for test C-20. Again, what can be appreciated is the effect of a higher chamber pressure, as the flame in test C-20 appears to be thicker and brighter. Moreover, the flame developing on the side and on the layer of melted paraffin between the slab and the window is more accentuated, as the melting of the surface layer is enhanced by the increased heat transfer given by the higher chamber pressure.

To summarize, the small increase in chamber pressure from atmospheric to a chocked condition fostered a transition in the observed behaviour of the combustion, as the flame moved from a thin flame core, typical of the ignition transient phase, to a more developed and more turbulent profile. Also, the pressure range appears to be too low to be neglected on the burning rate of the solid fuel, a results that is in accordance with literature.[14] The pressure conditions investigated are therefore still too low to be representative of a typical HRE combustion chamber.

DOI: 10.13009/EUCASS2023-041



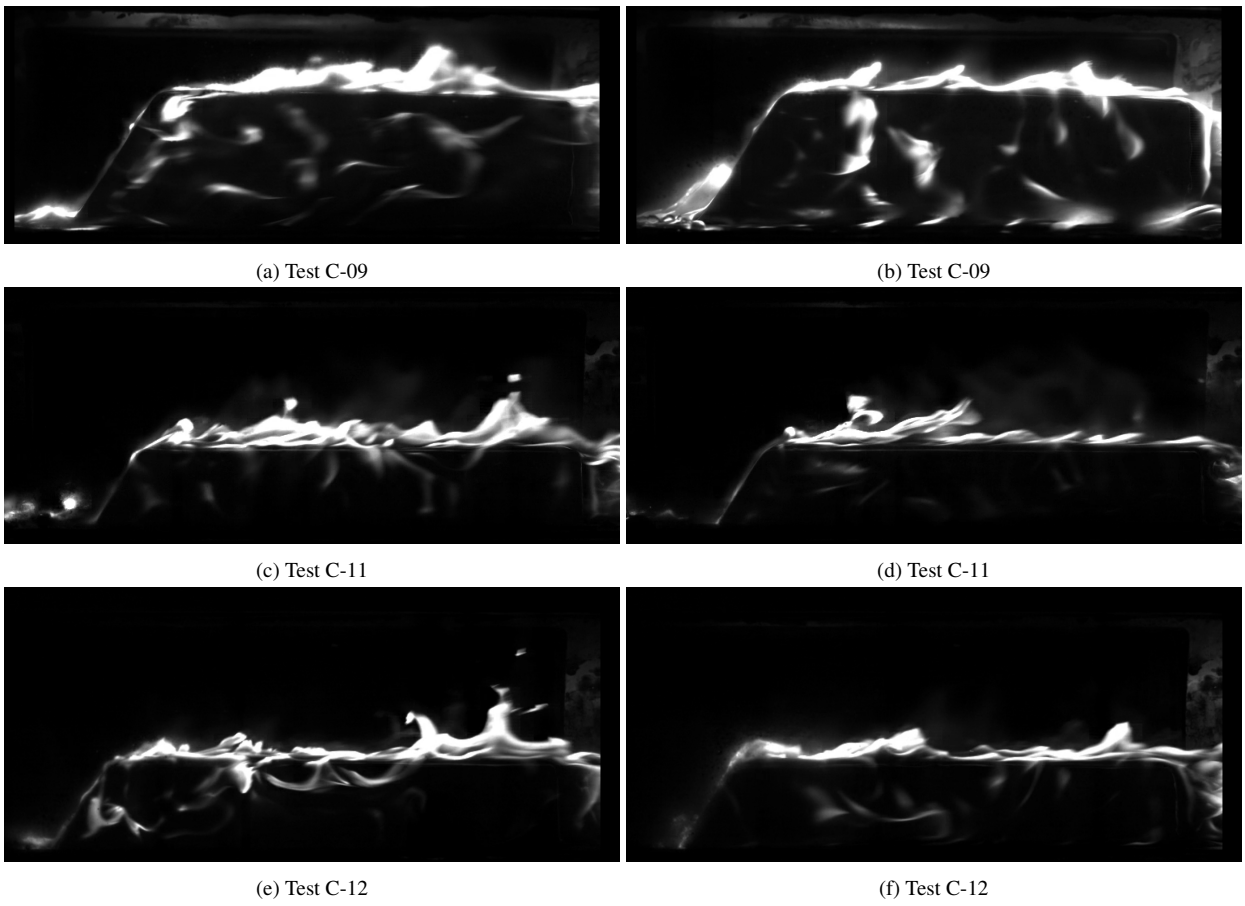

(a) Test C-09 (b) Test C-09

(c) Test C-11 (d) Test C-11

(e) Test C-12 (f) Test C-12

Figure 13: Paraffin combustion of Tests C-09, C-11 and C-12

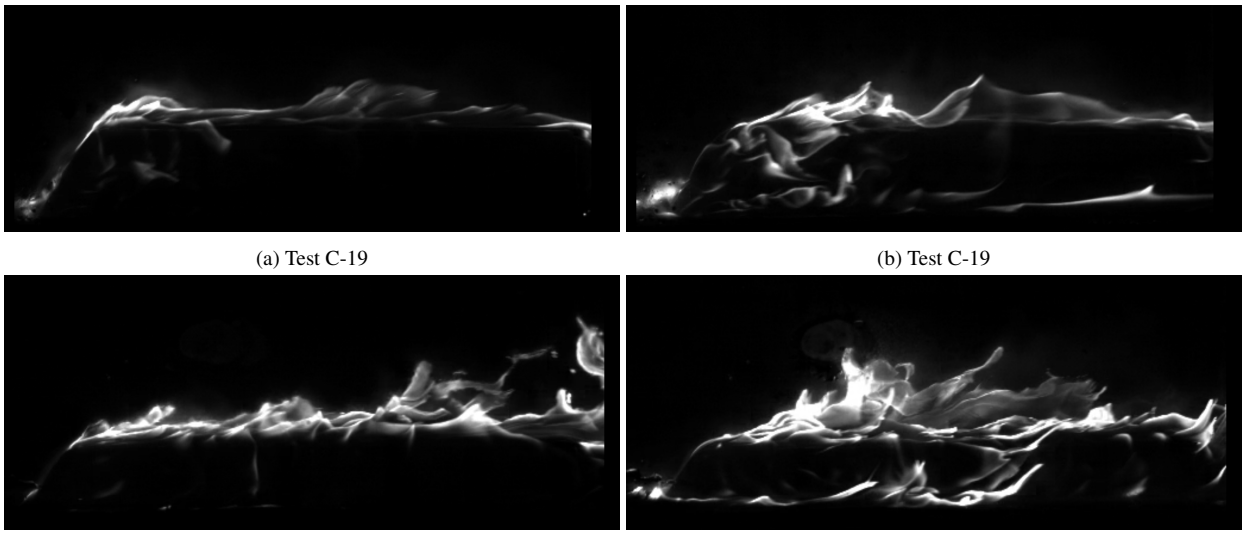

(a) Test C-19 (b) Test C-19

(c) Test C-20 (d) Test C-20

Figure 14: Paraffin combustion of Tests C-19 and C-20

### 3.5 High Pressure Tests

The third couple of tests discussed are Test 08 and 12, which both have a higher mass flow rate and mass flux with respect to the previous experiments, of around 29 kg/m$^2$, as well as a higher average combustion chamber pressure, between 9 bar for Test 08 and 10 for Test 12 (see Table 6), getting closer to the conditons experienced in a HRE. Some

DOI: 10.13009/EUCASS2023-041



images are shown in Figures 15 and 16. Some features of the combustion which appears at higher chamber pressures and mass flux are a much more developed flame, which tends to be thicker and brighter when compared with the previous tests, for the higher entrainment of paraffin in the oxidizer flow. The flame develops easily also on the side of the slab, and presents wave-like structures which couple with some pressure oscillations, generating a highly turbulent flame and local strong blowing effects with consequent ejection of paraffin droplets, as also discussed previously.

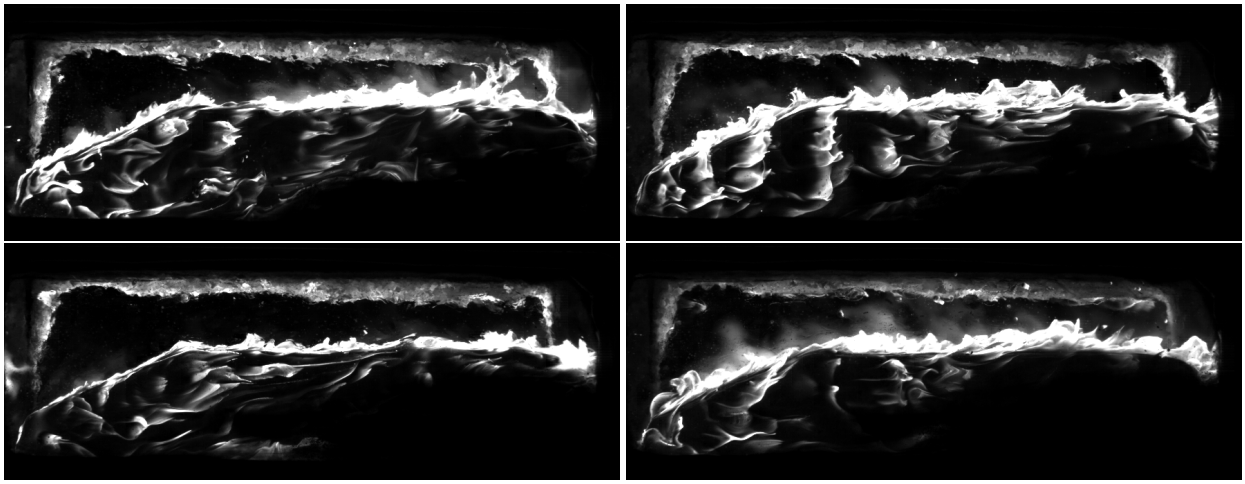

Figure 15: Paraffin combustion of Test 08

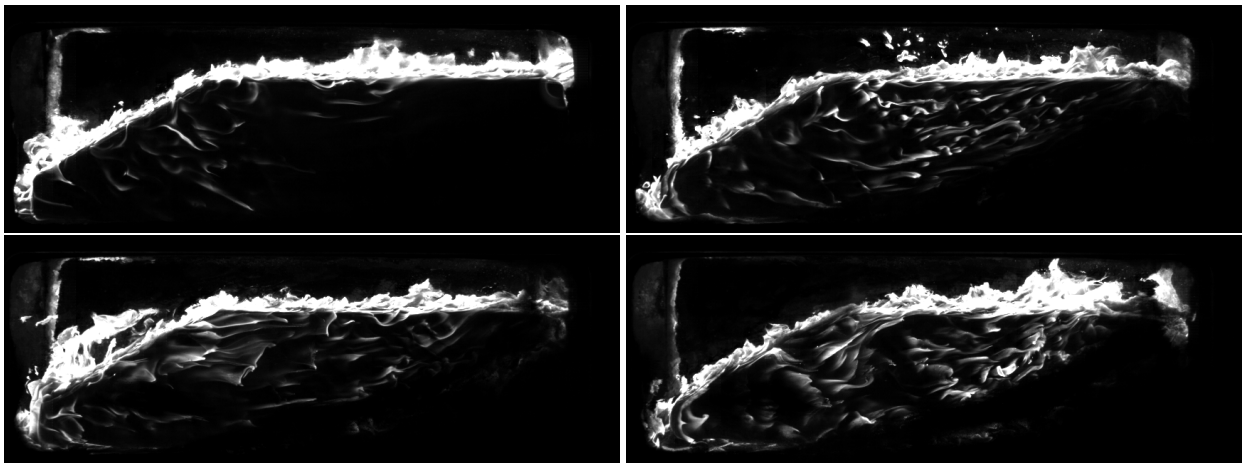

Figure 16: Paraffin combustion of Test 12

The last test discussed in this paper is Test 11. While it has not been considered in the test overview, as a steady operation point could not be achieved, is taken into account to analyse the transition to another different combustion behaviour which has been observed. The pressure in the test raised to 15 bar, when a safety switch in the test data acquisition and control system closed the oxygen valve to stop the combustion and depressurize the chamber. The test has been done in the same nominal conditions later achieved in Test 12, with an expected combustion chamber pressure of 10 bar. The explanation for the sudden pressure increase is due to the slab detachment from its support during the combustion, exposing a larger surface to the flow of oxygen. This increase of burning area increased the fuel mass flow injected in the chamber reaching a more efficient oxygen to fuel ratio, achieving a higher flame temperature and increasing the pressure in the chamber. The transition to the higher pressure combustion is shown in some frames in Figure 17. What can be observed is a larger and brighter flame core, which quickly saturates the camera sensor. This may be related to the higher flame temperature and also to a larger quantity of paraffin entrained in the oxidizer flow, as suggested by the large number of burning droplets and filaments that can be observed in the upper side of the flame, in the more oxidizer rich sector. The number of unsteady blowing events also increased, in accordance with what has been observed in literature.[2,15] Moreover, the turbulent flame structures that can be observed on the side of the slab becomes smaller in size, faster and more intense. This change of behaviour might be attributed to the transition of paraffin combustion from a subcritical to a supercritical phase, as the critical pressure of paraffin should be around 7 to

DOI: 10.13009/EUCASS2023-041



8 bar, depending on the exact formulation. This burning conditions therefore seems to be more representative of what should happen in the combustion chamber of a HRE, and may try to be further investigated in future works.

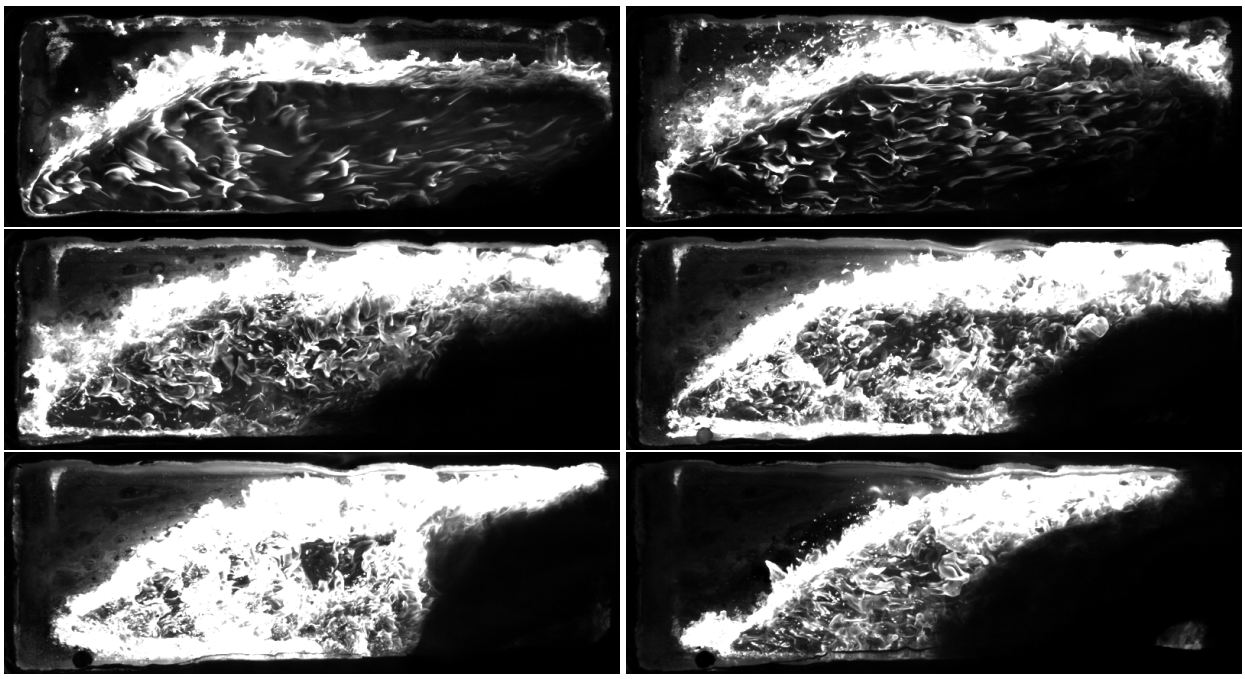

Figure 17: Paraffin combustion of Test 11

## 4. Conclusions

A hybrid rocket slab burner has been developed to study the combustion behaviour of solid fuels when burning with gaseous oxygen at different combustion chamber pressure and oxidizer mass flux. Two test campaigns have been carried out with the burner, in particular with paraffin fuels, and high-speed videos of the combustion have been recorded taking advantage of the optical access present in the combustor test section. This paper describes qualitatively the main features of paraffin combustion that have been observed at different test conditions and with different fuel grains, with the objective of giving an introduction to the different combustion behaviours observed at different experimental conditions. In particular, the commissioning tests videos acquired show a very similar behaviour between the tests, as low pressures have been tested. More interesting results have been acquired for the tests conducted in the Phase 2 test campaign, as different operating conditions have been set, observing the behaviour of paraffin combustion at atmospheric pressure and at higher chamber pressure, and the difference in the recorded videos assessed qualitatively. Moreover, a test at a higher pressure has been reported as well, where a change in the flame thickness, brightness and in the turbulence scale has been observed from the videos. Further research will start from the acquired images to move towards a quantitative analysis of the results. In particular, the objective is to identify the evolution of the flame thickness and brightness according to difference operating conditions, as well as the flow velocity and heat release. and to further expand the work on regression rate measurements from the videos. Moreover, additional tests will be executed to achieve a broader spectrum of operating conditions that can be investigated.

## 5. Acknowledgments

The authors would like to thank the technicians of the Aero-Thermo-Mechanics Department of Université Libre de Bruxelles for their support with the tests, in particular Charly, Florent and Lionel. We thank Christophe Vandevelde, Fabrice Tonnoir and Lindsey Couvrer (Laboratory for Energetic Materials, Royal Military Academy) for providing the high-speed camera, and the 1st Wing of the Air Component of the Belgian Armed Forces for hosting our test bench in the Beauvechain Air Base. We thank Anna Petrarolo (German Aerospace Center) for the guidance in the slab burners world. The research lies within the framework of the ASCenSIon project. The project leading to this application has received funding from the European Union's Horizon 2020 research and innovation programme under

DOI: 10.13009/EUCASS2023-041



the Marie Skłodowska-Curie grant agreement No 860956. A. E. De Morais Bertoldi received funding from the Marie Skłodowska-Curie grant agreement No 801505.

## References

[1] S. Kim, J. Lee, H. Moon, H. Sung, J. Kim, and J. Cho, "Effect of paraffin-ldpe blended fuel on the hybrid rocket motor," in *46th AIAA/ASME/SAE/ASEE Joint Propulsion Conference & Exhibit*, p. 7031, 2010.

[2] E. T. Jens, V. A. Miller, and B. J. Cantwell, "Schlieren and oh* chemiluminescence imaging of combustion in a turbulent boundary layer over a solid fuel," *Experiments in Fluids*, vol. 57, no. 3, pp. 1–16, 2016.

[3] E. T. Jens, A. C. Karp, V. A. Miller, G. S. Hubbard, and B. J. Cantwell, "Experimental visualization of hybrid combustion: results at elevated pressures," *Journal of Propulsion and Power*, vol. 36, no. 1, pp. 33–46, 2020.

[4] I. Nakagawa and S. Hikone, "Study on the regression rate of paraffin-based hybrid rocket fuels," *Journal of Propulsion and Power*, vol. 27, no. 6, pp. 1276–1279, 2011.

[5] A. Petrarolo, M. Kobald, and S. Schlechtriem, "Understanding kelvin–helmholtz instability in paraffin-based hybrid rocket fuels," *Experiments in Fluids*, vol. 59, no. 4, pp. 1–16, 2018.

[6] A. Petrarolo, M. Kobald, and S. Schlechtriem, "Visualization of combustion phenomena in paraffin-based hybrid rocket fuels at super-critical pressures," in *2018 Joint Propulsion Conference*, p. 4927, 2018.

[7] C. Paravan, R. Bisin, S. Carlotti, F. Maggi, and L. Galfetti, "Diagnostics for entrainment characterization in liquefying fuel formulations," in *2018 Joint Propulsion Conference*, p. 4663, 2018.

[8] L.-l. Liu, T.-y. Zhang, Z.-b. Chen, X. He, and Z. Ji, "Boundary layer combustion of paraffin fuels for hybrid propulsion applications," *Acta Astronautica*, vol. 193, pp. 338–345, 2022.

[9] R. Gelain, F. Angeloni, A. E. De Morais Bertoldi, and P. Hendrick, "Design and commissioning of the mouette hybrid rocket slab burner," in *9th European Conference for Aeronautics and Space Sciences (EUCASS)*, 2022.

[10] R. Gelain, A. Petrarolo, O. Assenmacher, A. E. De Morais Bertoldi, A. Rüttgers, and P. Hendrick, "Estimation of regression rate from image analysis in hybrid rocket slab burners," in *13th International Symposium on Special Topics in Chemical Propulsion and Energetic Materials*, 2023.

[11] A. Petrarolo, M. Kobald, and S. Schlechtriem, "Optical analysis of the liquid layer combustion of paraffin-based hybrid rocket fuels," *Acta Astronautica*, vol. 158, pp. 313–322, 2019.

[12] C. Glaser, J. Hijlkema, and J. Anthoine, "Evaluation of regression rate enhancing concepts and techniques for hybrid rocket engines," *Aerotecnica Missili & Spazio*, vol. 101, no. 3, pp. 267–292, 2022.

[13] A. Rüttgers, A. Petrarolo, and M. Kobald, "Clustering of paraffin-based hybrid rocket fuels combustion data," *Experiments in Fluids*, vol. 61, pp. 1–17, 2020.

[14] G. P. Sutton and O. Biblarz, *Rocket propulsion elements*. John Wiley & Sons, 2016.

[15] E. T. Jens, A. A. Chandler, B. Cantwell, G. S. Hubbard, and F. Mechentel, "Combustion visualization of paraffin-based hybrid rocket fuel at elevated pressures," in *50th AIAA/ASME/SAE/ASEE Joint Propulsion Conference*, p. 3848, 2014.